

Growth mechanism of catalyst- and template-free group III-nitride nanorods

Yong Sun Won^{a,b,*}, Young Seok Kim^a, Olga Kryliouk^{a,c,2,*}, Timothy J. Anderson^a

^a Department of Chemical Engineering, University of Florida, Gainesville, FL 32611-6005, USA

^b Samsung Electro-Mechanics Co. Ltd., Central R&D Institute, Suwon, Gyunggi-Do 443-743, Republic of Korea

^c Applied Materials, Santa Clara, CA 95052, USA

ARTICLE INFO

Article history:

Received 2 May 2008

Accepted 23 May 2008

Communicated by R. Kern

Available online 3 July 2008

PACS:

31.15.E-

34.50.Lf

62.23.Hj

81.05.Ea

81.15.Gh

82.60.-s

Keywords:

A1. DFT calculation

A1. Phase equilibria

A3. Hydride vapor phase epitaxy

B2. Semiconducting III–V materials

ABSTRACT

A feasible mechanism for catalyst- and template-free group III-nitride nanorod growth by hydride vapor phase epitaxy (HVPE) is proposed. The mechanism is composed of random nanoparticle nucleation from stable gas-phase oligomers and subsequent directional growth along the *c*-axis. A combined study of equilibrium analysis and computational thermochemistry was employed to determine the optimum growth conditions—growth temperature and Cl/group III ratio—based on the proposed mechanism, and the computed values showed good agreement with reported experimental results. The involvement of a group III trichloride as a key species in the proposed mechanism required the Cl/group III ratio to be ~ 3 according to stoichiometry. A higher Cl/group III ratio led to etching of the solid phase and a lower ratio favored two-dimensional film growth instead. The zone of GaN and InN nanorod growth by HVPE was shown to lie in the vicinity of the growth–etch transition. A two-temperature approach, employed in GaN nanorod growth, was supported by the deconvolution of two conflicting kinetic and thermodynamic constraints in terms of growth temperature: a high-temperature region for GaCl₃ formation that is kinetically limited at low temperature and a low-temperature region for GaN nanorod growth without GaN etching that is thermodynamically favorable in a chlorinated environment at high temperature. The temperature for AlN nanorod growth by chemical vapor deposition using AlCl₃ and NH₃ was limited only by the thermodynamic constraint of ammonia adduct (Cl₃Al:NH₃) formation.

© 2008 Elsevier B.V. All rights reserved.

1. Introduction

Nanoscale structures (such as nanowires and nanorods, hereafter termed NRs) of group III-nitride materials have attracted extensive interest for applications in quantum electronics, optoelectronics, and sensors [1–8]. We have already demonstrated the promising application of Pt-coated InN NRs in hydrogen gas sensors [9]. In many cases, group III-nitride nanorods have been grown by catalyst-assisted and oxide-assisted vapor-phase growth techniques [10–14], whose growth mechanisms have been described by the vapor–liquid–solid mechanism and the vapor–solid mechanism involving a series of oxidation and reduction steps, respectively [14]. On the other hand, only limited success with catalyst-, oxide- and template-independent group III-nitride NR growth has been reported. Typically, GaN NR growth was achieved by hydride vapor phase epitaxy (HVPE) [15], InN NR growth by hydride metal organic vapor phase epitaxy (H-MOVPE)

[9,16], and AlN NR growth occurred by chemical vapor deposition (CVD) using AlCl₃ and NH₃ [17]. Complete growth mechanisms have thus not yet been proposed.

Meanwhile, several theoretical studies of potential gas-phase intermediates in group III-element (Al, Ga, and In)-N-H-Cl systems suggested formation of thermodynamically stable oligomer species, [Cl₂(Al, Ga or In)NH₂]_n, in the gas phase, even at elevated temperatures up to 1000 K [18–21]. Timoshkin also pointed out earlier the possibility of gas-phase nanoparticle formation in his theoretical study on the stability of rings and clusters in the gas phase during CVD of group III–V materials [22]. On the basis of those conclusions [18–22], we introduced a probable solid–vapor mechanism for InN NR growth by H-MOVPE, featuring random nanoparticle nucleation from stable gas-phase oligomers and subsequent directional growth along the *c*-axis, in our previous report [16,23]. Experimental observations were fairly consistent with the proposed growth mechanism [16].

In this study, the proposed solid–vapor mechanism [16,23] is rationalized in more detail, using equilibrium analysis combined with computational thermochemistry. The optimum growth conditions for group III-nitride (InN, GaN, and AlN) NR growth are determined by evaluating the kinetic and thermodynamic constraints on the system. Growth conditions determined by computation are then compared with experimental results

* Corresponding authors at: Department of Chemical Engineering, University of Florida, Gainesville, FL 32611-6005, USA.

E-mail addresses: yongsun.won@samsung.com (Y.S. Won),

Olga_Kryliouk@amat.com (O. Kryliouk).

¹ Tel.: +82 31 2106731; fax: +82 31 3007900(9695#).

² Tel.: +1 408 235 6033.

reported in literature [15–17] to verify the mechanism, particularly the growth temperature and Cl/Group III ratio, which were found to be the most influential growth parameters [16].

2. Computational methods

All computational thermochemistry calculations were carried out using GAUSSIAN 03 with B3LYP DFT model chemistry and a split basis set (LanL2DZ for the element In and 6-311G(d) for other elements) [24–26]. Full geometry optimization was carried out for all gas species. The transition state (TS) was located using the Berny algorithm, as implemented in GAUSSIAN 03 [24]. Harmonic vibration frequencies were calculated for each structure, which allowed the enthalpy and Gibbs energy to be obtained computationally.

The CVD phase diagrams were computed using ThermoCalc software with the SUB94 database implemented in the software [27–30].

3. Results and discussion

3.1. Growth mechanism of group III-nitride nanorods

The mechanism of catalyst- and template-free group III-nitride NR growth, for the case of InN NR growth by H-MOVPE, is proposed in Fig. 1 [16,23]. In this modified HVPE system, HCl reacts with trimethylindium (TMIn) instead of the liquid indium source used in conventional HVPE [16]. The unique idea of this proposed mechanism is the possibility of nucleation of nanoparticles from stable gas-phase oligomer species ($[\text{Cl}_2\text{InNH}_2]_n$ in Fig. 1). The oligomer is an aggregate of the monomer (Cl_2InNH_2 in Fig. 1) with HCl eliminated from the ammonia adduct ($\text{Cl}_3\text{In:NH}_3$ in Fig. 1).

As shown in Fig. 1, two-dimensional film growth initiated with uniform nucleation by the surface reaction of adsorbed InCl and NH_3 is favored when the Cl/group III ratio is ~ 1 . In this regime,

InCl (more generally, a group III monochloride) is the dominant gas-phase reactant species, accompanied by NH_3 . When the Cl/group III ratio is increased to 3, formation of a group III trichloride (InCl_3 in Fig. 1) becomes kinetically feasible, provided that the growth temperature is greater than 800 K, but negative entropy ($\Delta S < 0$) makes it thermodynamically unfavorable with increasing temperature. This conflicting temperature dependency is discussed in Sections 3.2 and 3.3. The group III trichloride (InCl_3) then forms an ammonia adduct ($\text{Cl}_3\text{In:NH}_3$) by reaction with NH_3 and subsequent HCl elimination leads to a monomer (Cl_2InNH_2) having an innate group III–N bond [18–22]. The oligomer species (more generally, $[\text{Cl}_2(\text{Al, Ga or In})\text{NH}_2]_n$), an aggregate of monomers, has been identified as stable in the gas phase below a certain temperature (up to 1000 K) [18–22]. Strong intramolecular H–Cl hydrogen bonding and dipole–dipole interactions are known to favor formation of larger oligomer species [20]. The extent of oligomerization has not been determined experimentally, but Timoshkin reported in his theoretical works that the generation of gas-phase $[\text{HGaNH}]_n$ clusters even with oligomerization degree $n \geq 60$ was viable [31,32]. When the Cl/group III ratio becomes much higher than 3, group III-nitride growth becomes unfavorable as a result of enhanced etching by excess gaseous HCl. In addition, equilibrium of the reaction ($\text{InCl}_3\text{:NH}_3 \leftrightarrow \text{Cl}_2\text{InNH}_2 + \text{HCl}$ in Fig. 1) shifts against monomer formation. The result is either sparse nucleation or a complete lack of growth.

The growth mechanism proposed in Fig. 1 was used to describe the growth behavior observed in InN NR growth by H-MOVPE [16]. The involvement of a group III trichloride (InCl_3) as a key intermediate in the mechanism requires that the Cl/group III ratio be ~ 3 according to stoichiometry and it was confirmed that the optimum Cl/In ratio was 3–4 [16]. Using higher Cl concentrations (Cl/In = 4–7), sparse nanorods or micro-rods were grown [16]. The growth behavior of InN NRs was independent of the substrate (silicon, GaN, or sapphire) [16]. This follows from the idea that nucleation of nanoparticles from gas-phase oligomers is unlikely to be dependent on the substrate surface.

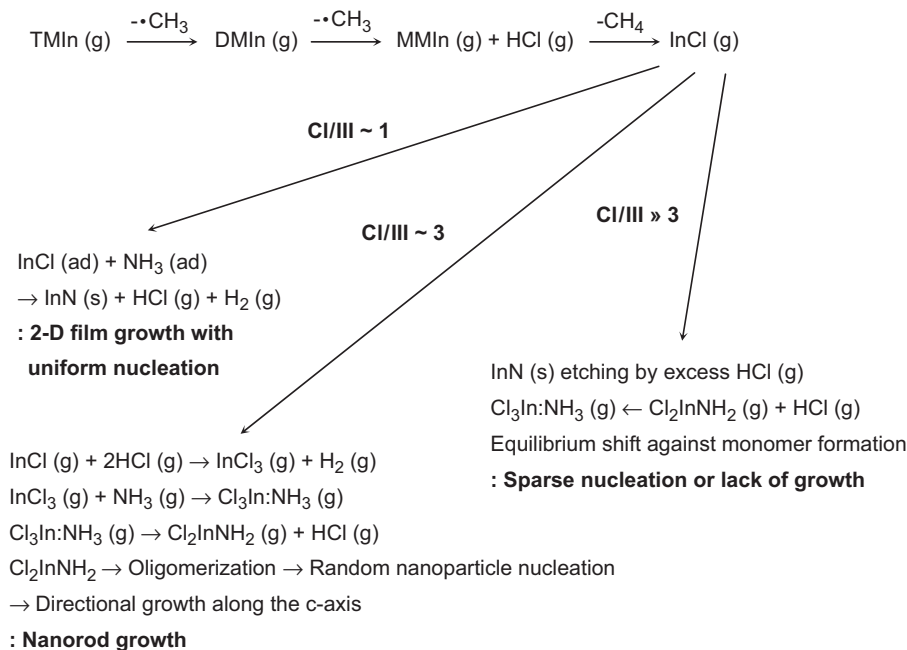


Fig. 1. Growth mechanism of group III-nitride NRs for the case of InN NR growth by H-MOVPE [23].

The observations that an individual NR was faceted, without any cap morphology, and its diameter did not change along the growth direction (*c*-axis) suggested that a solid–vapor mechanism, initiated by random nanoparticle nucleation and subsequent directional growth, was in operation [16]. Preferential growth along the *c*-axis [15–17] can be explained by dipole–dipole interactions between nanoparticles and gas-phase precursor species. An oligomer species ($\text{Cl}_9\text{Ga}_6\text{N}_6\text{H}_9$) [21], for example, has the wurtzite structure inside although its boundaries are saturated with hydrogen and chlorine atoms. Thus, the nanoparticle nucleated from this kind of oligomer species has its dipole axis along the *c*-axis of its incorporated wurtzite structure. The dipole axis of each nanoparticle is likely to be oriented randomly at the initial stage of nucleation on the substrate surface. Chlorine-containing gas-phase precursor species also have strong dipoles, as does NH_3 . Therefore, higher reactant flux driven by dipole–dipole interactions on the NR end would favor directional growth along the *c*-axis on each NR. The experimental results demonstrated that the growth rate along the *c*-axis was significantly higher than the rate in the lateral direction [15–17]. It has also been demonstrated that preferential growth of ZnO NRs in plasma-enhanced CVD occurred along the *c*-axis in the presence of a perpendicular electric field by attracting charged particles to the NR ends [33]. Initial random orientation of the nanoparticle dipole axes resulted in the randomly oriented final NR structure [15–17].

3.2. Gas-phase kinetics

The growth temperature and Cl/group III ratio were confirmed experimentally as key growth parameters [16]. While the desirable Cl/group III ratio for NR growth was determined to be ~ 3 by the ideas inherent in the proposed growth mechanism (see Fig. 1), a combination of computational thermochemistry and equilibrium analysis was employed to locate the most preferable temperature range for NR growth based on the proposed mechanism. The results are discussed in Sections 3.2 and 3.3. The growth temperature in CVD was often determined by kinetically limited gas-phase reactions. Thus, the detailed computational thermochemistry study was used to obtain activation barriers for gas-phase reactions and evaluate the kinetic constraints of the system in terms of growth temperature.

To test the selected basis set of moderate size (LanL2DZ for In element and 6-311G(d) for other elements), reaction enthalpies for the thermal decomposition process $\text{TMIIn} \rightarrow \text{dimethylindium (DMIn)} \rightarrow \text{monomethylindium (MMIn)}$, which occurs initially in H-MOVPE [16], were calculated and compared with literature values [34] obtained using a larger basis set as shown in Table 1. The results show that the selected basis set describes the trend of enthalpies for the methyl dissociation from TMIIn with fair accuracy. The higher enthalpy value for the decomposition of trimethylgallium (TMGa) compared to that of TMIIn at each step is consistent with experimental reports as well [35]. Note that the second methyl dissociation (entries 2 and 5 in Table 1) has a much lower energy barrier and would occur rapidly, as has been reported in the literature [35]. The DMIn and dimethylgallium (DMGa) have the planar doublet C_{2v} geometry with an unpaired electron due to their sp^2 hybridization and they are likely to decompose readily to stable singlet MMIn and monomethylgallium (MMGa), where one electron in the p orbital is in effect donated to the carbon. The Mulliken atomic charges of In and C elements (In/C) were varied in DMIn and MMIn as follows: 0.601/–0.196 (DMIn) \rightarrow 0.445/–1.069 (MMIn). The MMIn and MMGa are stabilized by the ionic characteristics of In–C and Ga–C bonds. The energy barriers for the third methyl dissociation from MMIn

Table 1
Calculated reaction enthalpies for the thermal decomposition of TMIIn and TMGa

Entry	Reactions	ΔH_{298}° calculated (kcal/mol)	ΔH_{298}° in literature (kcal/mol)
1	$\text{In}(\text{CH}_3)_3 \rightarrow \text{In}(\text{CH}_3)_2^+ \cdot \text{CH}_3$	61.1 ^a	58.8 ^b
2	$\text{In}(\text{CH}_3)_2 \rightarrow \text{InCH}_3^+ \cdot \text{CH}_3$	26.6 ^a	24.7 ^b
3	$\text{InCH}_3 \rightarrow \text{In}^+ \cdot \text{CH}_3$	54.0 ^a	53.8 ^b
4	$\text{Ga}(\text{CH}_3)_3 \rightarrow \text{Ga}(\text{CH}_3)_2^+ \cdot \text{CH}_3$	70.8	–
5	$\text{Ga}(\text{CH}_3)_2 \rightarrow \text{GaCH}_3^+ \cdot \text{CH}_3$	33.5	–
6	$\text{GaCH}_3 \rightarrow \text{Ga}^+ \cdot \text{CH}_3$	60.0	–

^a Data was taken from Ref. [23].

^b Data was taken from Ref. [33].

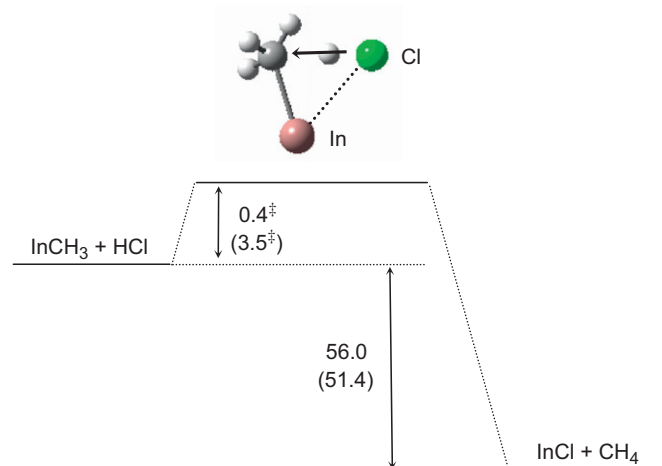


Fig. 2. Calculated energetics of the formation of InCl [23] and GaCl. The ΔU_{298}° and $\Delta U_{298}^{\ddagger}$ values have the unit of kcal/mol and values in parenthesis are for the GaCl formation.

and MMGa increase again as a result of strong In–C and Ga–C bonds.

The formation of InCl (or GaCl) by reaction of MMIn (or MMGa) with HCl, which is known to occur in H-MOVPE, is depicted in Fig. 2. The calculated energetics shows a low barrier for the reaction and its high exothermicity shifts the reaction forward. The main gas species, with Cl/group III ratio ~ 1 , would thus become InCl (or GaCl). Two-dimensional film growth then follows via the surface reaction between adsorbed InCl (or GaCl) and NH_3 . In HVPE, liquid In (or Ga) reacts with HCl to form InCl (or GaCl).

When the Cl/group III ratio increases to 3, another pathway becomes viable in the gas phase, by formation of group III trichloride. Fig. 3 illustrates the calculated energetics of InCl_3 (or GaCl_3) formation from InCl (or GaCl) by reaction with two HCl molecules. The overall reaction is exothermic with negative ΔS , meaning that the pathway becomes thermodynamically unfavorable above a certain temperature, which is discussed in Section 3.3. This pathway had a relatively high activation barrier for the first HCl insertion to form InHCl_2 (or GaHCl_2), probably due to the change in bond characteristics from ionic to sp^2 hybridized. InHCl_2 (or GaHCl_2) and InCl_3 (or GaCl_3) have planar C_{2v} and C_{3h} symmetry resulting from sp^2 hybridization, respectively.

The formation of ammonia adducts ($\text{Cl}_3\text{In}:\text{NH}_3$, $\text{Cl}_3\text{Ga}:\text{NH}_3$, and $\text{Cl}_3\text{Al}:\text{NH}_3$) readily follows as a result of the high exothermicity of those reactions. Table 2 lists calculated reaction enthalpies for the

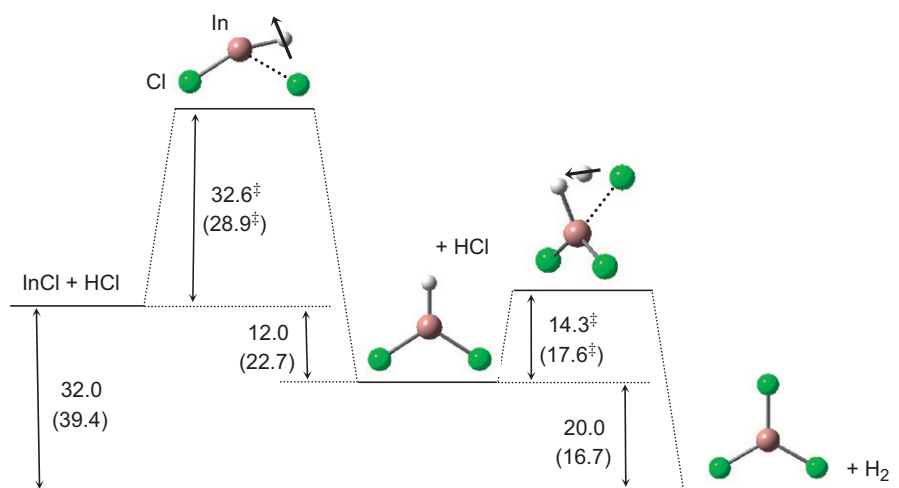


Fig. 3. Calculated energetics of the formation of InCl_3 [23] and GaCl_3 . The $\Delta U_{298}^{\ddagger}$ and $\Delta U_{298}^{\ddagger}$ values have the unit of kcal/mol and values in parenthesis are for the GaCl_3 formation.

Table 2

Reaction enthalpies for the formation of ammonia adducts ($\text{Cl}_3\text{In}:\text{NH}_3$, $\text{Cl}_3\text{Ga}:\text{NH}_3$, and $\text{Cl}_3\text{Al}:\text{NH}_3$); Calculated and literature values

Reactions	ΔH_{298}° calculated (kcal/mol)	ΔH_{298}° in literature (kcal/mol)
$\text{InCl}_3 + \text{NH}_3 \rightarrow \text{Cl}_3\text{In}:\text{NH}_3$	-36.9 ^a	-35.9 ^b
$\text{GaCl}_3 + \text{NH}_3 \rightarrow \text{Cl}_3\text{Ga}:\text{NH}_3$	-39.0	-37.2 ^b
$\text{AlCl}_3 + \text{NH}_3 \rightarrow \text{Cl}_3\text{Al}:\text{NH}_3$	-41.6	-42.2 ^b

^a Data was taken from Ref. [23].

^b Data was taken from Ref. [19].

ammonia adduct formation and corresponding literature values obtained using a higher level MP2 theory [19], which showed good agreement. Although subsequent monomer formation through HCl elimination is endothermic, the enthalpy of reaction is smaller than the energy gained in the corresponding ammonia adduct formation, regardless of the group III element [19]. This suggests that HCl elimination can easily occur in the gas phase as long as the ammonia adduct formation is thermodynamically and kinetically favorable. Okamoto [19] reported that the activation energy for the monomer formation is 'not much larger than the reaction energy' and Timoshkin et al. [20] found that the TS for HCl elimination from $\text{GaCl}_3:\text{NH}_3$ lies only at 1 kJ/mol (SCF/pVDZ level) higher than the reaction energy.

In summary, there are two kinetically limited gas-phase reaction steps in the proposed mechanism (see Fig. 1), namely the first methyl dissociation from TMIIn (or TMGa) and the first HCl insertion into InCl (or GaCl) to form InHCl_2 (or GaHCl_2). The former is limited by the large bond dissociation energy shown in Table 1, while the latter is a bimolecular reaction (two moles of reactants \rightarrow one mole of TS, $\Delta S^{\ddagger} < 0$) having a fairly high activation energy (Fig. 3). Table 3 summarizes the values of $\Delta G^{\circ,\ddagger}$ and rate constants of those reactions at several different temperatures. The absolute rate equations from transition state theory (TST) were used for the calculation of rate constants as shown below [36]. For the simple dissociation and insertion where no obvious TSs exist (entries 1/3 and 4/6), it was assumed $\Delta H^{\circ} = \Delta H^{\circ,\ddagger}$ and $\Delta S^{\circ} = \Delta S^{\circ,\ddagger}$:

$$k_{\text{unimolecular}} = (k_{\text{B}}T/h) \exp(-\Delta G^{\circ,\ddagger}/RT)$$

$$k_{\text{bimolecular}} = (k_{\text{B}}T/h)(RT/P^{\circ}) \exp(-\Delta G^{\circ,\ddagger}/RT)$$

where k_{B} , h , and R are the Boltzmann constant, Planck constant, and gas constant, respectively, and $P^{\circ} = 1$ atm.

Although rate constants listed in Table 3 are not suitable for rigorous analysis, they demonstrate that a high temperature (HT, > 800 K) is required for the two kinetically limited reactions (entries 1/2 and 4/5), especially HCl insertion into InCl , to have significant rate constants and be kinetically accessible. Ammonia adduct formation (entry 3/6) was shown to be facile, even at HT, because of the exothermicity ($\Delta H_{298}^{\circ} < 0$) of this reaction, despite its high negative entropy generation ($\Delta S_{298}^{\circ} < 0$).

3.3. Temperature dependency of group III-nitride NR growth

In Section 3.2, we discussed the kinetic constraint that HT (> 800 K) is required to activate the formation of InCl_3 as a key species in the proposed growth mechanism. However, this conflicts with the high degree of group III-nitride etching observed in a chlorinated environment at HT, especially for InN and GaN . A CVD phase diagram for GaN growth with $\text{Cl}/\text{group III}$ ratio versus growth temperature is presented in Fig. 4(a). The growth region shrank rapidly with increasing Cl/Ga ratio and growth temperature. Although higher N/Ga ratios expanded the growth region at higher Cl/Ga ratios, the degree of GaN etching in a chlorinated environment was generally considerable. For a Cl/Ga ratio around three, the phase transition temperature ranged 600–650 K, which is apparently not high enough for the activation of GaCl_3 formation. The kinetic constraint requiring HT and the thermodynamic constraint requiring low temperature (LT) are in conflict here.

A two-temperature approach is thus suggested to deconvolute the two conflicting constraints: a combination of a HT region for GaCl_3 formation and a LT region for GaN NR growth. The upper temperature limit of the HT region could be determined by the thermodynamic favorability of GaCl_3 formation, because it has a negative entropy generation. Table 4 summarizes the calculated $\Delta G^{\circ}(T)$ values for the InCl_3 and GaCl_3 formation reactions and the temperatures where their signs change. The lower temperature limit of the HT region is determined by the kinetic constraint (> 800 K) of GaCl_3 formation, as discussed in Section 3.2. The upper temperature limit of the LT region follows the phase diagram shown in Fig. 4(a). Kim et al. [15] demonstrated a similar two-temperature approach (750 °C for precursor mixing and 480 °C for NR growth) for catalyst- and template-free GaN NR growth by HVPE.

The degree of InN etching in a chlorinated environment is even higher. Recent data from Leitner et al. [37] with well-supported

Table 3
Calculated activation energies and rate constants for selected reactions at several different temperatures

Entry	Reactions	$\Delta S_{298}^{\ddagger}$ (cal/mol-K)	$\Delta H_{298}^{\ddagger}$ (kcal/mol)	$\Delta G_{298}^{\ddagger}/k$ ^a 298 K	$\Delta G_{298}^{\ddagger}/k$ ^a 800 K	$\Delta G_{298}^{\ddagger}/k$ ^a 1300 K
1 ^b	$\text{In}(\text{CH}_3)_3 \rightarrow \text{In}(\text{CH}_3)_2 + \text{CH}_3$	37.8	61.1	$49.8/1.8 \times 10^{-25}$	$31.0/5.6 \times 10^{+5}$	$13.0/1.8 \times 10^{+12}$
2 ^b	$\text{InCl} + \text{HCl} \rightarrow [\text{InCl} \cdots \text{HCl}]^{\ddagger}$	-26.5	32.0	$39.9/2.1 \times 10^{-15}$	53.2/3.2	$66.2/2.1 \times 10^{+5}$
3 ^b	$\text{InCl}_3 + \text{NH}_3 \rightarrow \text{Cl}_3\text{In} \cdots \text{NH}_3$	-33.3	-36.9	$-26.9/3.5 \times 10^{+33}$	$-10.7/1.4 \times 10^{+17}$	$4.3/5.2 \times 10^{+13}$
4	$\text{Ga}(\text{CH}_3)_3 \rightarrow \text{Ga}(\text{CH}_3)_2 + \text{CH}_3$	38.2	70.8	$59.4/1.6 \times 10^{-30}$	$40.3/1.6 \times 10^{+3}$	$22.0/5.4 \times 10^{+10}$
5	$\text{GaCl} + \text{HCl} \rightarrow [\text{GaCl} \cdots \text{HCl}]^{\ddagger}$	-26.9	28.3	$36.4/3.3 \times 10^{-12}$	$49.9/2.5 \times 10^{+2}$	$63.2/6.7 \times 10^{+5}$
6	$\text{GaCl}_3 + \text{NH}_3 \rightarrow \text{Cl}_3\text{Ga} \cdots \text{NH}_3$	-35.5	-39.0	$-28.4/4.5 \times 10^{+34}$	$-11.2/1.9 \times 10^{+17}$	$5.0/3.9 \times 10^{+13}$

^a ΔG^{\ddagger} values have the unit of kcal/mol. The rate constants have the unit of s^{-1} for the unimolecular reaction and $\text{L mol}^{-1} \text{s}^{-1}$ for the bimolecular reaction.
^b Data were taken from Ref. [23].
^c Transition state.

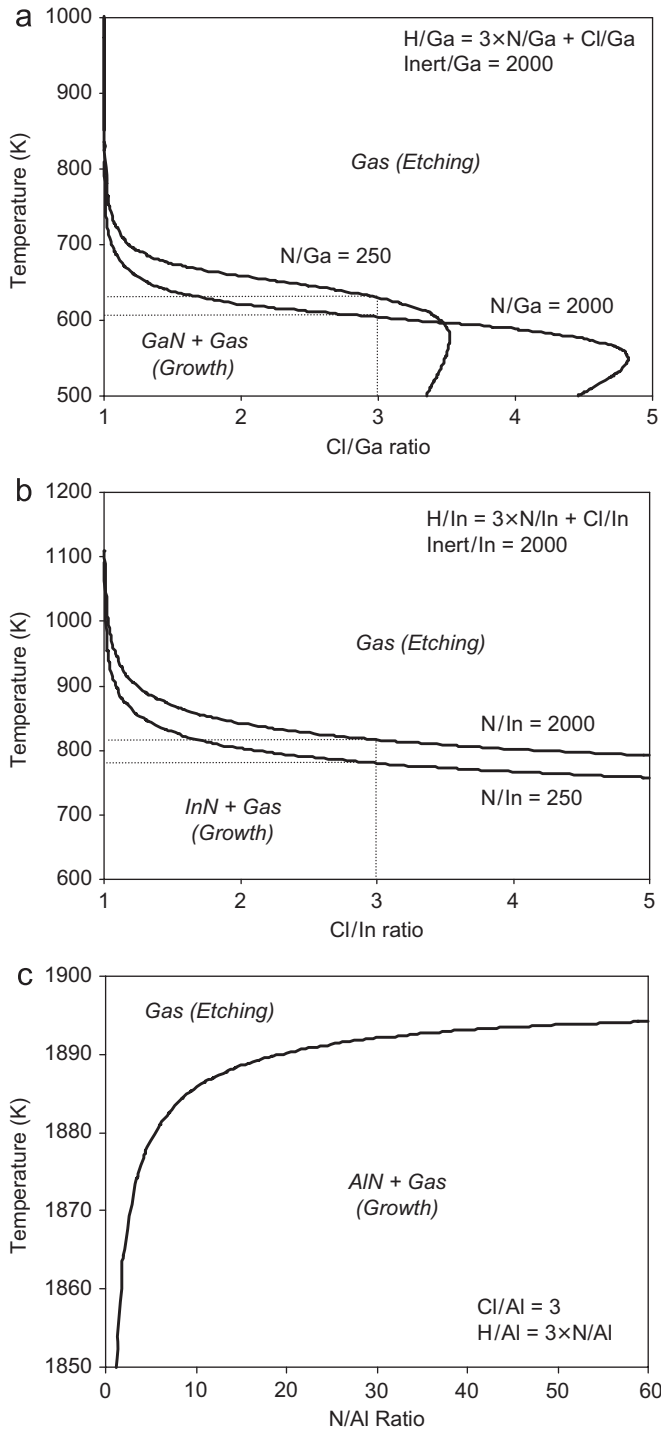


Fig. 4. CVD phase diagram for (a) GaN, (b) InN [23], and (c) AlN growth.

Table 4
Calculated Gibbs energies for the formation of InCl_3 and GaCl_3 at specified temperatures

Reactions	ΔG° (kcal/mol)			T (K) $\Delta G^\circ(T) = 0$
	298 K	800 K	1300 K	
$\text{InCl}(\text{g}) + 2\text{HCl}(\text{g}) \leftrightarrow \text{InCl}_3(\text{g}) + \text{H}_2(\text{g})$	-22.9 ^a	-7.6 ^a	6.6 ^a	1070 ^a
$\text{GaCl}(\text{g}) + 2\text{HCl}(\text{g}) \leftrightarrow \text{GaCl}_3(\text{g}) + \text{H}_2(\text{g})$	-29.9	-13.9	1.1	1260

^a Data were taken from Ref. [23].

experimental results showed that thermal decomposition of solid InN (~680 K) occurs below the typical growth temperature (~800 K) of InN films [37,38]. Thus, InN NR growth by H-MOVPE [16] was apparently achieved under nonequilibrium conditions, because the thermodynamic constraint does not allow formation of InN at the temperature used (~900 K). The CVD phase diagram in Fig. 4(b) matches the growth behaviors observed in InN NR growth by H-MOVPE fairly well, as shown in our previous report [16]. The Gibbs energy for solid InN was taken from the ThermoCalc SUB94 database. This corresponds to reducing the Gibbs energy by ~16 kcal/mol relative to the value given in Leitner et al. It still needs a bit more decrease of the Gibbs energy of InN(s) to fit the experimental results exactly. Reducing the Gibbs energy of InN(s) in Fig. 4(b) could be understood as consideration of the kinetic barrier for decomposition since the decomposition and growth temperatures generally overlap because of kinetic barriers. Note also that the optimum temperature for InN NR growth was confined to the very narrow range of 600–650 °C (873–923 K) [16]. Considering that InN film growth using the same H-MOVPE system—where InCl is dominant in the gas phase—was possible at temperatures as low as 500–550 °C (773–823 K) [38], the temperature range of 600–650 °C was likely determined by the kinetic constraint of InCl_3 formation (see Table 3). The high degree of InN etching (thermodynamic constraint) contained the growth temperature within the narrow range, where the kinetic constraint is barely removed. Increasing the N/In ratio increased the phase transition temperature at a given Cl/In ratio. The growth zone of GaN and InN NRs by HVPE, however, was generally in the vicinity of the growth–etch transition as reported in our previous work [16,23].

The controlled growth of AlN NR arrays by CVD was recently reported by Yang et al. [17] using the volatile compound AlCl_3 and NH_3 at 950 °C. The CVD phase diagram for AlN growth, with N/Al ratio versus growth temperature at fixed Cl/Al = 3, shown in Fig. 4(c), demonstrates that the etching of AlN in a chlorinated environment was not important compared to that of GaN and InN. The AlN growth was possible up to a fairly HT (~1880 K) without etching even in a low-nitrogen environment (N/Al ratio ~5). Thus, only the upper temperature limit of AlN NR growth is determined

Table 5
Calculated Gibbs energies for the formation of $\text{Cl}_3\text{Al}:\text{NH}_3$ at specified temperatures

Reactions	ΔG° (kcal/mol)			T (K)
	298 K	800 K	1300 K	
$\text{AlCl}_3(\text{g})+\text{NH}_3(\text{g})\leftrightarrow\text{Cl}_3\text{Al}:\text{NH}_3(\text{g})$	−30.9	−13.5	2.9	1210

by the thermodynamic constraint of ammonia adduct ($\text{Cl}_3\text{Al}:\text{NH}_3$) formation, because it has a negative entropy generation. The $\Delta G^\circ(T)$ values calculated for various temperatures, and summarized in Table 5, set the upper limit for growth temperature of AlN NRs at ~ 1210 K (937°C). As discussed in Section 3.2, the subsequent monomer (Cl_2AlNH_2) formation consumed lesser energy than was gained via ammonia adduction formation.

4. Conclusions

A probable mechanism for catalyst- and template-independent group III-nitride nanorod growth in HVPE, comprising random nanoparticle nucleation from stable gas-phase oligomers and subsequent directional growth along the c -axis, was proposed. The growth conditions determined by computation on the basis of the proposed mechanism agreed well with reported experimental results.

Computational thermochemistry was employed to locate kinetic constraints for gas-phase reactions ranging from decomposition of group III organometallic precursors to ammonia adduct formation. A HT (> 800 K) is needed to kinetically activate the formation of group III trichloride, a key species in the proposed mechanism. However, equilibrium analysis presented a conflicting thermodynamic constraint attributed to the high degree of group III-nitride (especially InN and GaN) etching in a chlorinated environment at HT. Thus, a two-temperature approach was suggested to deconvolute the two conflicting constraints: combination of a HT region to activate the group III-trichloride formation and a LT region for NR growth without etching. The temperature dependency of InN and GaN NR growth was shown to be determined by the growth–etch transition. For AlN NR growth, the growth temperature was not limited by etching, but by the thermodynamic constraint of ammonia adduct formation. The important role of group III trichloride in the proposed mechanism required a preferable Cl/group III ratio of ~ 3 .

References

- [1] J. Sánchez-Páramo, J. Calleja, M. Sánchez-García M, M. Calleja, *Physica E* 13 (2002) 1070.
- [2] E. Calleja, M. Sánchez-García, F. Sánchez, F. Calle, F. Naranjo, E. Muñoz, U. Jahn, K. Ploog, *Phys. Rev. B* 62 (2002) 16826.
- [3] J. Ristic, E. Calleja, M. Sánchez-García, F. Ulloa, J. Sánchez-Páramo, J. Calleja, U. Jahn, A. Trampert, K. Ploog, *Phys. Rev. B* 68 (2003) 125305.

- [4] J. Wang, M.S. Gudiksen, X. Duan, Y. Cui, C.M. Lieber, *Science* 293 (2001) 1455.
- [5] J.C. Johnson, H.J. Choi, K.P. Knutsen, R.D. Schaller, P. Yang, R.J. Saykally, *Nature* 1 (2002) 106.
- [6] L.J. Lauhon, M.S. Gudiksen, D. Wang, C.M. Lieber, *Nature* 420 (2002) 57.
- [7] S. Dhara, A. Datta, C.T. Wu, Z.H. Lan, K.H. Chen, Y.L. Wang, L.C. Chen, C.W. Hsu, H.M. Lin, C.C. Chen, *Appl. Phys. Lett.* 82 (2003) 451.
- [8] J.W. Chiou, J.C. Han, H.M. Tsai, W.F. Pong, M.H. Tsai, I.H. Hong, R. Klausner, J.F. Lee, C.W. Hsu, C.C. Chen, C.H. Shen, L.C. Chen, K.H. Chen, *Appl. Phys. Lett.* 82 (2003) 3949.
- [9] O. Kryliouk, H.J. Park, H.T. Wang, B.S. Kang, T.J. Anderson, F. Ren, S.J. Pearton, *J. Vac. Sci. Technol. B* 23 (5) (2005) 1891.
- [10] X.F. Duan, C.M. Lieber, *J. Am. Chem. Soc.* 122 (2000) 128.
- [11] C.H. Liang, C.L. Chen, J.S. Hwang, K.H. Chen, Y.T. Hung, Y.F. Chen, *Appl. Phys. Lett.* 19 (2004) 423.
- [12] H.Y. Peng, X.T. Zhou, N. Wang, Y.F. Zheng, L.S. Liao, W.S. Shi, C.S. Lee, S.T. Lee, *Chem. Phys. Lett.* 327 (2000) 263.
- [13] M.K. Sunkara, S. Sharma, R. Miranda, G. Lian, E.C. Dickey, *Appl. Phys. Lett.* 79 (2001) 1546.
- [14] C.N.R. Rao, F.L. Deepak, G. Gundiah, A. Govindaraj, *Prog. Solid State Chem.* 31 (2003) 5.
- [15] H.M. Kim, D.S. Kim, Y.S. Park, D.Y. Kim, T.W. Kang, K.S. Chung, *Adv. Mater.* 14 (13–14) (2002) 991.
- [16] O. Kryliouk, H.J. Park, Y.S. Won, T.J. Anderson, A. Davydov, I. Levin, J.H. Kim, J.A. Freitas Jr., *Nanotechnology* 18 (13) (2007) 135606.
- [17] J. Yang, T.W. Liu, C.W. Hsu, L.C. Chen, K.H. Chen, C.C. Chen, *Nanotechnology* 17 (2006) S321.
- [18] A.Y. Timoshkin, H.F. Bettinger, H.F. Schaefer III, *J. Am. Chem. Soc.* 119 (1997) 5668.
- [19] Y. Okamoto, *J. Crystal Growth* 191 (1998) 405.
- [20] A.Y. Timoshkin, H.F. Bettinger, H.F. Schaefer III, *Inorg. Chem.* 41 (2002) 738.
- [21] A. Kovács, *Inorg. Chem.* 41 (2002) 3067.
- [22] A.Y. Timoshkin, H.F. Schaefer III, *Chem. Rec.* 2 (2002) 319.
- [23] Y.S. Won, Y.S. Kim, O. Kryliouk, T.J. Anderson, *Phys. Stat. Sol. C* 5 (6) (2008) 1633.
- [24] M.J. Frisch, G.W. Trucks, H.B. Schlegel, G.E. Scuseria, M.A. Robb, J.R. Cheeseman, J.A. Montgomery Jr., T. Vreven, K.N. Kudin, J.C. Burant, J.M. Millam, S.S. Iyengar, J. Tomasi, V. Barone, B. Mennucci, M. Cossi, G. Scalmani, N. Rega, G.A. Petersson, H. Nakatsuji, M. Hada, M. Ehara, K. Toyota, R. Fukuda, J. Hasegawa, M. Ishida, T. Nakajima, Y. Honda, O. Kitao, H. Nakai, M. Klene, X. Li, J.E. Knox, H.P. Hratchian, J.B. Cross, V. Bakken, C. Adamo, J. Jaramillo, R. Gomperts, R.E. Stratmann, O. Yazyev, A.J. Austin, R. Cammi, C. Pomelli, J.W. Ochterski, P.Y. Ayala, K. Morokuma, G.A. Voth, P. Salvador, J.J. Dannenberg, V.G. Zakrzewski, S. Dapprich, A.D. Daniels, M.C. Strain, O. Farkas, D.K. Malick, A.D. Rabuck, K. Raghavachari, J.B. Foresman, J.V. Ortiz, Q. Cui, A.G. Baboul, S. Clifford, J. Cioslowski, B.B. Stefanov, G. Liu, A. Liashenko, P. Piskorz, I. Komaromi, R.L. Martin, D.J. Fox, T. Keith, M.A. Al-Laham, C.Y. Peng, A. Nanayakkara, M. Challacombe, P.M.W. Gill, B. Johnson, W. Chen, M.W. Wong, C. Gonzalez, J.A. Pople, *Gaussian 03, Revision C 02*, Gaussian, Inc., Wallingford CT, 2004, p. 26.
- [25] A.D. Becke, *J. Chem. Phys.* 98 (1993) 1372.
- [26] P.J. Stephens, F.J. Devlin, C.F. Chabalowski, M.J. Frisch, *J. Phys. Chem.* 98 (1994) 11623.
- [27] B. Sundman, B. Janson, J.O. Anderson, *Thermochem* 9 (1985) 153.
- [28] I. Barin, *Thermochemical Data of Pure Substances*, VCH, Weinheim, 1989.
- [29] O. Kubaschewski, C.B. Alcock, P.J. Spencer, *Materials Thermochemistry*, Pergamon Press, Oxford, 1996.
- [30] J.M.W. Chase, (Ed.), *NIST-JANAF Thermochemical Tables*, fourth ed., American Chemical Society and the American Institute of Physics, New York, 1999.
- [31] A.Y. Timoshkin, H.F. Schaefer III, *J. Am. Chem. Soc.* 126 (2004) 12141.
- [32] A.Y. Timoshkin, H.F. Bettinger, H.F. Schaefer III, *J. Phys. Chem. A* 105 (2001) 3240.
- [33] X. Liu, X. Wu, H. Cao, R.P.H. Chang, *J. Appl. Phys.* 95 (6) (2004) 3141.
- [34] B.H. Cardelino, C.E. Moore, C.A. Cardelino, D.O. Frazier, K.J. Bachmann, *J. Phys. Chem. A* 105 (2001) 849.
- [35] G.B. Stringfellow, *Organometallic Vapor-Phase Epitaxy: Theory and Practice*, second ed., Academy Press, San Diego, 1999, p. 215.
- [36] C.J. Cramer, *Essentials of Computational Chemistry*, Wiley, Chichester, 2002.
- [37] J. Leitner, P. Marsik, D. Sedmidubsky, K.J. Ruzicka, *Phys. Chem. Solids* 65 (2004) 1127.
- [38] S.W. Kang, H.J. Park, Y.S. Won, O. Kryliouk, T.J. Anderson, D. Khokhlov, T. Burbaev, *Appl. Phys. Lett.* 90 (2007) 112616.